INCREASING THE PARAMETER ROBUSTNESS OF ACTIVE CONTOURS USING IMAGE DATA DRIVEN INITIALIZATIONS

K. Ohliger[1]*, T. Edeler*[1]*, S. Hussmann*[1] *and A. Mertins*[2]

[1]Institute Ma.Vi.Tec,Westcoast University Heide
D-25746 Heide, Germany
Email: ohliger@fh-westkueste.de

[2]Institute for Signal Processing,
University of Lübeck
D-23562 Lübeck, Germany

ABSTRACT

Although the well-known task of image segmentation which partitions the image into separated areas including different objects is part of almost every image processing application it still remains challenging. In the early 90's level set methods became a popular framework for front propagation methods like active contours (ACs) including edge-based and region-based models. Due to the optimization in a local manner those methods lead to segmentation results which depend on the initialization. While edge-based models are commonly known to be very sensitive to the initialization in noisy and realistic images, the initializing of region-based models are expected to be much more robust to varying initialization. In this paper we investigate the parameter robustness of different edge-based models concerning different initializations for synthetic and real images containing Gaussian noise with different noise levels. We show that the robustness of region-based ACs can be significantly increased by image data driven initializations. We compare the segmentation results of different models on synthetic and real images with respect to the Dice coefficient.

1. INTRODUCTION

The partitioning of an image into different areas which contain different objects of the scene is the task of image segmentation. Although it has to be done in nearly every application including image processing, it remains challenging and is still part of actual research. The approach of image segmentation using front propagation was first introduced as *Snakes* by Kass et al. [1] in 1988. This model resulted in an energy functional which includes an external energy term driving the contour to large image gradients and an internal energy regarding the contours length and stiffness. *Snakes* were successfully used in different applications (see [2, 3, 4, 5]) despite several drawbacks, such as the inability of allowing topological changes, noise sensitivity and strong dependency on the initialization (cf. [6]).

In [7] Osher and Sethian introduced a level set formalism which is able to allow topological changes. Casselles et al. [8] and Malladi et al. [9] integrated this formalism for image segmentation applications. As written in [6] the problem of solving the energy functional still remains a local optimization problem and the initialization has significant influence of the resulting segmentation for many realistic images.

In 1996 Zhu and Yuille introduced a novel approach using region-based active contours (ACs) considering segmentation as probabilistic partitioning problem in [10] and Chan and Vese combined this approach with the level set methods in [11]. As written in [6] region-based ACs are expected to be more independent on the initialization and more robust against noise.

To our best knowledge there exist no comparative study concerning the influence of different initialization methods for region-based ACs using level sets to the parameter robustness of level set methods in noisy images. In [12, 13] we showed that segmentation using region-based ACs are sensitive to initializations.

The outline of this paper is as follows: In Section 2 we introduce our image model and in Section 3 we give a brief introduction into the initialization methods we take into account for our experimental results. The basic idea of region-based ACs is shown in Section 4 and in the subsequent sections we will introduce the region-based methods used for evaluation. After introducing the level set algorithm and its parameters in Section 5 we provide experimental results for synthetic and real images containing different amount of noise in Section 6. Section 7 finalizes this paper with conclusions.

Ma.Vi.Tec is supported by the European Union (EFRE) and the federal state of Schleswig-Holstein, Germany (Zukunftsprogramm Wirtschaft)

2. IMAGE MODEL

The image model that we use is strongly related to the model introduced in [13]. Let $u_0 : L_x \times L_y \rightarrow \mathbb{R}$ the undistorted image with $L_x = \{1, 2, \ldots, N_x\}$ and $L_y = \{1, 2, \ldots, N_y\}$. We assume that u_0 contains $N \in [2, N_x \cdot N_y]$ objects ω_j with $j \in [1, N]$:

$$u_0(k,l) = \sum_{i=1}^{N} f_{\omega_j}(k,l) \tag{1}$$

for $k \in [1, N_x]$ and $l \in [1, N_y]$. The function f_{ω_j} is determined by

$$f_{\omega_j}(k,l) = \begin{cases} F_j(k,l) & k,l \text{ inside of } \omega_j \\ 0 & \text{otherwise} \end{cases}, \tag{2}$$

with

$$\mathbf{F}_j \sim N\left(\mu_{\omega_j}, \sigma^2_{\omega_j}\right). \tag{3}$$

Extending the model with additive independent identically distributed Gaussian noise $N\left(0, \sigma^2_N\right)$ which leads to the distorted image $\tilde{u}_0$ by substition of $\mathbf{F}_j$ in (2) by $\tilde{\mathbf{F}}_j$ with

$$\tilde{\mathbf{F}}_j \sim N\left(\mu_{\omega_j}, \sigma^2_{\omega_j} + \sigma^2_N\right). \tag{4}$$

3. INITIALIZATION METHODS

Initialization methods (IMs) for ACs can be divided into data independent initializations (DIIs) which take no image data into account and the data driven initializations (DDIs) which initialize the ACs by

analyzing the image content. In Sections 3.1 and 3.2 we introduce the different IMs compared in this work. We point out that we do not focus on developing new initialization methods but on comparing DIIs with DDIs.

3.1. Data Independent Initializations (DIIs)

The most common IMs for initialization of ACs are data independent initializations, namely enveloping initialization (EI) and regular grid initialization (RGI). For EI a circle with radius r_{EI} or a square with side length w_{EI} is placed centered on the image. r_{EI} or w_{EI} are chosen to envelop most of the image (cf. [11, 14]). For the RGI small circles with radius r_{RGI} or squares with width w_{RGI} are placed in a regular grid with pitch d_{max} on the image for the initial contours (ICs) with $d_{max} > 2 \cdot r_i$ or $d_{max} > w_i$ respectively (cf. [15, 16]).

3.2. Data Driven Initializations (DDIs)

Up to now there exist just few data driven initializations. If the DIIs fail it is common to use manual initializations if possible. Further DDIs are introduced in our previous works [12, 13]. In this work we use for data driven initializations a modified RGI (MRGI) which just includes circles which are located on the same object.

4. REGION-BASED ACTIVE CONTOURS

This section gives a short introduction into region-based ACs followed by detailed informations of the different region-based methods used in this work.
As written in [15] and [6] region-based ACs can be derived from the Bayes rule expressing the conditional probability p for partition P of the image plane $\mathbf{\Omega}$ for a given image $\mathbf{U}$:

$$p\left(P(\mathbf{\Omega})\left|\mathbf{U}\right.\right) \propto p\left(\mathbf{U}|P(\mathbf{\Omega})\right) \cdot p\left(P(\mathbf{\Omega})\right) . \tag{5}$$

The first term denotes the likelihood including the image based impact (data dependent term) and the second term is the prior containing image independent information of which partition is more likely (smoothing term). The prior is often chosen to prefer short contour length $|C|$:

$$p\left(P(\mathbf{\Omega})\right) \propto e^{-\nu|C|} \tag{6}$$

with ν being a positive weighting constant. Taking the widely used assumption into account, that pixels within each region are independent, the likelihood can be expressed as:

$$p\left(\mathbf{U}|P(\mathbf{\Omega})\right) = \prod_{i=1}^{N} p\left(\mathbf{U}|\Omega_i\right) , \tag{7}$$

with $\mathbf{\Omega} = \{\Omega_1, \ldots \Omega_N\}$. Maximization of (5) is equivalent to minimizing of

$$E\left(\mathbf{\Omega}\right) = -\sum_{i=1}^{N} \left[\sum_{k,l \in \Omega_i} \ln p_i\left(u\left(k,l\right)\right) \right] + \nu\left|C\right| , \tag{8}$$

while p_i is the probability density function (PDF) of region Ω_i. If the partition of the image is accurate and Ω_i equals the area containing ω_i only, $p_i = p_{\omega_j}$ which is the PDF of $\tilde{\mathbf{F}}_j$.

4.1. Chan and Vese (CV)

A special case for region-based ACs is the energy definition based on a two phase piecewise constant model introduced by Chan and Vese in [11]. The functional (8) changes to:

$$E\left(\mathbf{\Omega}\right) = -\sum_{i=1}^{2} \left[\lambda_i \sum_{k,l \in \Omega_i} \left|u\left(k,l\right) - c_i\right|^2 \right] + \nu\left|C\right| + \mu \sum_{k,l \in \Omega_1} , \tag{9}$$

with Ω_1 enveloped by the contour C. As recommended by the authors we choose $\lambda_1 = \lambda_2 = 1$ and additionally we set $\mu = 0$ to be comparable to the other region-based ACs. Doing this (9) can be derived from (8) for p_i being a unimodal gaussian distribution and $\sigma_1 = \sigma_2$. The values of c_i are determined by

$$c_i = \frac{\sum\limits_{k,l \in \Omega_i} u\left(k,l\right)}{\sum\limits_{k,l \in \Omega_i}} . \tag{10}$$

4.2. Parametric Region-Based (RB)

In order to minimize (8) an estimation of the unknown PDFs p_i is required. In many applications ([10, 17, 18]) p_i is assumed to be a unimodal Gaussian distribution

$$\tilde{p_i} \sim N\left(\mu_{\Omega_i}, \sigma^2_{\Omega_i}\right) , \tag{11}$$

with μ_{Ω_i}, $\sigma^2_{\Omega_i}$ being the empirical mean and variance of region Ω_i respectively.

4.3. Nonparametric Region-Based (NRB)

Estimating $\tilde{p_i}$ in a nonparametric manner for region-based ACs is seldom and only few literature exist (cf. [19, 20]). We use in this paper the nonparametric density estimation based on histograms as it was done by Comaniciu et al. in [21]:

$$\tilde{p}_{i,hist}\left(I\right) = \frac{\sum\limits_{k,l \in \Omega_i} X\left(u\left(k,l\right), I\right)}{\sum\limits_{\Omega_i}} , \tag{12}$$

with $I = \{I_{min}, I_{min} + \Delta_I, \ldots, I_{max}\}$ and

$$X\left(\tilde{I}, I\right) = \begin{cases} 1 & I - 0.5\Delta_I \leq \tilde{I} < I + 0.5\Delta_I \\ 0 & \text{otherwise} . \end{cases} \tag{13}$$

5. LEVEL SET ALGORITHM

Since their introduction in 1988 level sets have become very popular and simultaneously many level set algorithms of different types have been developed. They differ in representation of the curve (implicitly or explicitly), update domain (global or narrow band) or segmentation type (two phase or multiphase). An overview is given by Shi and Karl in [22]. We decided to choose an algorithm which has an implicit representation of the curve with a narrow band updating domain for two phase segmentation. The used algorithm is the real-time algorithm for curve evolution introduced by Shi and Karl in [22]. This algorithm uses four different parameters, namely N_g, N_a, N_s and σ. While N_g and σ control the size and bandwidth of the smoothness done by Gaussian filtering, N_a is the count of evolution steps driven by the data dependent term, and N_s the count of evolution steps driven by the smoothing term. Due to the fact that N_g controls only the size of the Gaussian filter its influence is negligible for the segmentation result, if its size is chosen to be at least $3 \cdot \sigma_{max}$.

6. EXPERIMENTAL RESULTS

In this Section we provide experimental results for the segmentations depending on the initializations, parameters of the level set algorithm, and different kind of images including varying noise levels. The images were scaled to $[0, 1]$ before adding the noise. Due to the computational costs the images were chosen to have a maximum size of $128 \times 128\ px^2$. For all experiments the parameters of the level set algorithm were varying independently as follows:

- $\sigma = \{1, 1.5, \ldots, 5\}$ with $N_g = 15$

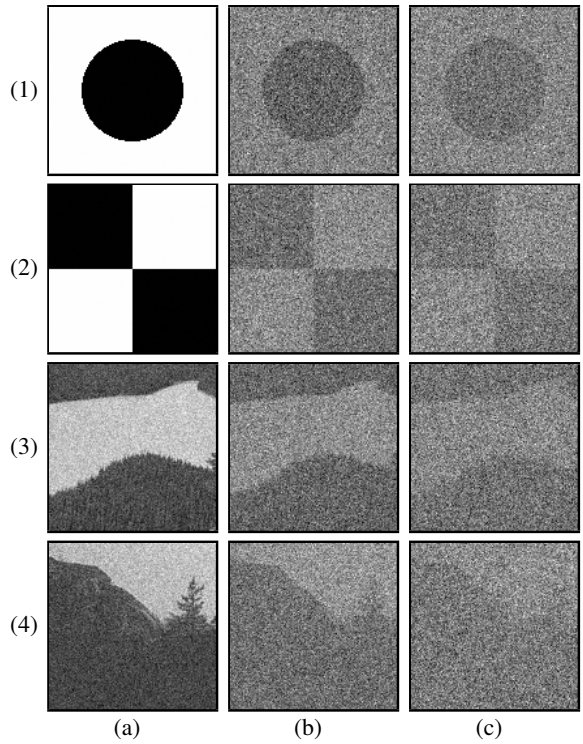

Fig. 1. Rows (1) to (2) show the synthetic images $\mathbf{U_{1,1}}$, $\mathbf{U_{2,1}}$ (a) respectively, $\mathbf{U_{1,2}}$, $\mathbf{U_{2,2}}$ (b) respectively, $\mathbf{U_{1,3}}$, $\mathbf{U_{2,3}}$ (c) respectively. Rows (3) to (4) show the real images $\mathbf{U_{3,1}}$, $\mathbf{U_{4,1}}$ (a) respectively, $\mathbf{U_{3,2}}$, $\mathbf{U_{4,2}}$ (b) respectively, $\mathbf{U_{3,3}}$, $\mathbf{U_{4,3}}$ (c) respectively.

- $N_a = \{10, 14, \ldots, 50\}$
- $N_s = \{1, 2, \ldots, 9\}$.

This lead to 891 segmentations for each image. The parameter ranges were chosen to provide accurate results for the mean values of the parameters. We compare the results of segmentations for the region-based methods CV, RB, and NRB using the different initializations EI, RGI, and MRGI with respect to the mean and variation of the Dice coefficient (see Section 6.1).

The different initializations used for the experiments are shown in Fig. 2. The EI initialization includes a circular region with $r_{EI} = 62px$. The RGI contains 81 circles with $r_{RGI} = 6px$ and $d_{max} = 14px$. The MRGI uses the same radius and pitch as the RGI but only circles containing the same object were considered. These initializations were equal for every noise level and every image.

6.1. Dice Coefficient (DC)

The quality of the segmentation result is determined by the Dice coefficient introduced by Dice in [23]

$$DC\left(\widetilde{\Omega_1}, \Omega_1\right) = \frac{2\left|\widetilde{\Omega_1} \cap \Omega_1\right|}{\left|\widetilde{\Omega_1}\right| + |\Omega_1|} \tag{14}$$

with $\widetilde{\Omega_1}$ being the segmented set of the respective algorithm and Ω_1 is the reference set. $|\cdot|$ denotes the cardinality of the set. The DC range is $[0, 1]$ while one indicates a perfect segmentation.

6.2. Synthetic Images

For the experiments in this work we created two different synthetic images, a circle and a quadrant image. They are shown in Rows (1) and (2) in Column (a) of Fig. 1. We added to the undistorted images $\mathbf{U_{1,1}}$ and $\mathbf{U_{2,1}}$ two different levels of noise $\sigma^2_{n,1} = 1$ and $\sigma^2_{n,2} = 2.25$ creating the images $\mathbf{U_{i,2}}$ and $\mathbf{U_{i,3}}$, respectively.

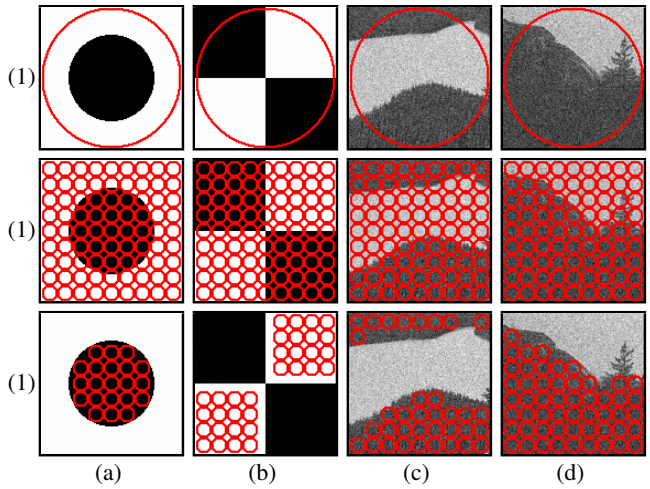

Fig. 2. Initializations for the different images. Column (a): circle image, Column (b): quadrant image, Column (c): river delta image, Column (d): panorama image. Row (1): EI with circular shape, Row (2): RGI with circular shape, Row (3): MRGI with circular shape.

The amount of brightness in the images of Fig. 3 is linear to the segmentation error. Black areas in the images are indicating correct segmentations while white areas have always been segmented wrong.

The images of Fig. 3 lead to the following results: It is obvious that the most common used initialization for CV, the EI seems to be more sensitive to parameter variation than using the RGI. The MRGI lead for CV in particular for the quadrant images to worse results than the RGI.

Using RB the result is different to CV as it is shown in the second block *Parametric Region-Based* of Fig. 3. The differences between EI and MRGI are negligible while RGI seems to be very sensitive to parameter variation.

The third block *Nonparametric Region-Based* of Fig. 3 shows that RGI and MRGI lead to similar results while MRGI performs slightly better for the quadrant image and RGI for the circle image respectively. The EI shows for the quadrant image very high sensitivity to the parameter variation. In Fig. 4 the DC PDFs for CV in (a), RB in (b), and NRB in (c) with all initialization variants for all images are shown. The diagrams show that MRGI performs best or similar to the best initialization method for RB and NRB with respect to the mean and variance of DC. For CV the performance of EI and MRGI are similar but they are outperformed by RGI.

6.3. Real Images

The experiments for evaluation of the parameter robustness for real images were done on two images which are supposed to fit our image model. The original images and there reference segmentation were selected from the Berkeley segmentation dataset[1]. We take these images as undistorted images although they contain noise due to the fact that they are real images. We crop a part of image *55067.jpg* and also from *176035.jpg* and converted both to gray level images $\mathbf{U_{3,1}}$ and $\mathbf{U_{4,1}}$ as shown in Rows (3) and (4) of Fig. 1. We added to the undistorted images $\mathbf{U_{3,1}}$ and $\mathbf{U_{4,1}}$ two different levels of noise $\sigma^2_{n,1} = 0.25$ and $\sigma^2_{n,2} = 1$ creating the images $\mathbf{U_{i,2}}$ and $\mathbf{U_{i,3}}$ which

[1] http://www.eecs.berkeley.edu/Research/Projects/CS/vision/bsds/

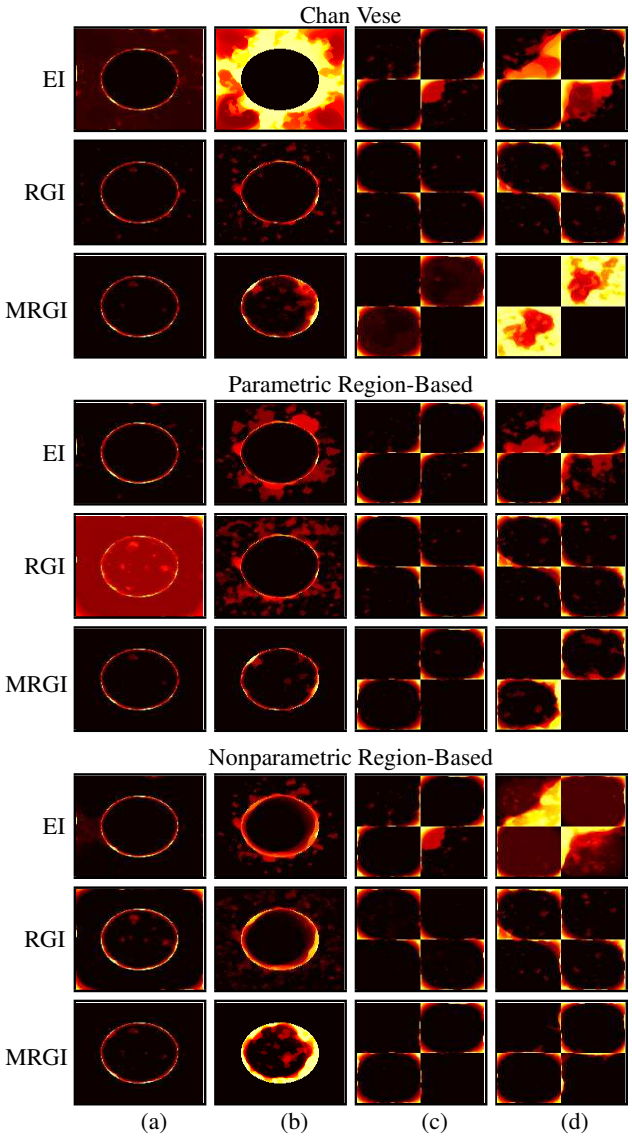

Fig. 3. Images showing the variation of the different methods and different initializations for $\mathbf{U_{1,2}}$, $\mathbf{U_{1,3}}$, $\mathbf{U_{2,2}}$, and $\mathbf{U_{2,3}}$ in Columns (a), (b), (c), and (d) respectively.

are shown in Columns (b) and (c) in Rows (3) and (4) of Fig. 1.
The images of Fig. 3 lead to the following results: The CV method performs best with the EI for all images with slightly better performance then RGI. The main difference to MRGI is the segmentation variation of image $\mathbf{U_{3,3}}$ where MRGI lead to worse results.
The RB method performs best with the EI with little advances to MRGI. The RGI lead to the worst performance in particular for the higher amount of noise in $\mathbf{U_{3,3}}$ and $\mathbf{U_{4,3}}$.
For the nonparametric region-based method the segmentation variation between the different initialization methods is similar for $\mathbf{U_{3,2}}$ and $\mathbf{U_{4,2}}$. For $\mathbf{U_{3,3}}$ RGI performs worst with very high segmentation variation and for $\mathbf{U_{4,3}}$ EI performs better than MRGI and RGi which perferms worst.

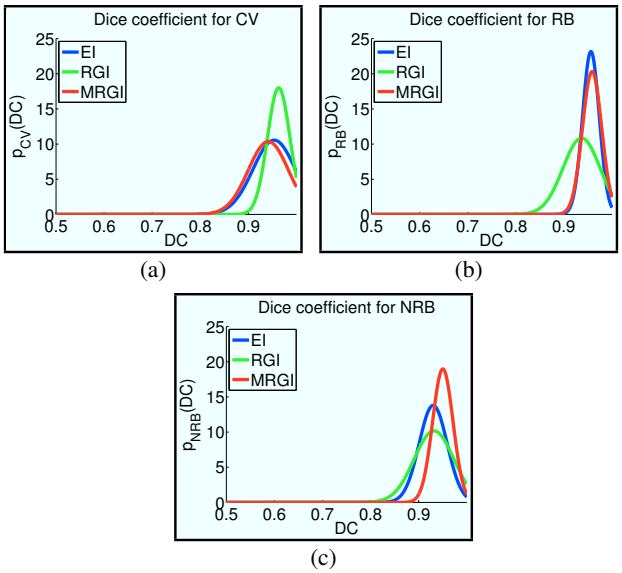

Fig. 4. Estimated DC PDFs for the different region-based methods and initializations based on 3564 segmentations.

7. CONCLUSIONS

In this paper we showed the impact of initialization for region-based active contours. We compare a data dependent initialization method, namely the modified regular grid initialization, with state of the art initialization methods, namely the enveloping initialization and regular grid initialization, which are data independent initializations. We take three different region-based active contours methods into account: the CV which is based on a piecewise constant model, the RB which uses parametric density estimations, and the NRB using nonparametric density estimations. Experimental results on synthetic and real images containing different noise levels showed that the CV method is much more robust to parameter variation using RGI than MRGI or EI. For the RB and NRB methods the MRGI performs best or with slightly differences to the respective best method.

8. REFERENCES

[1] M. Kass, A. Witkins, and D. Terzopoulus, "Snakes: active contour models," *Int. J. Comput. Vision*, vol. 1, no. 4, pp. 321–332, 1988.

[2] L. Cohen, "On active contour models and balloons," *CVGIP: Image understanding*, vol. 53, no. 2, pp. 211–218, 1991.

[3] I. Carlbom, D. Terzopoulos, and K. Harris, "Computerassisted registration, segmentation, and 3d reconstruction from images of neuronal tissue sections," *IEEE Trans. Med. Imag.*, vol. 13, no. 2, pp. 351–362, 1994.

[4] F. Leymarie and M. Levine, "Simulating the grassfire transform using an active contour model," *IEEE Trans. Pattern Anal. Mach. Intell.*, vol. 14, no. 1, pp. 158–175, 1995.

[5] R. Malladi and J. Sethian, "A real-time algorithm for medical shape recovery," *IEEE Trans. Pattern Anal. Mach. Intell.*, vol. 14, no. 1, pp. 158–175, 1995.

[6] D. Cremers, M. Rousson, and R. Deriche, "Review of statistical approaches to level set segmentation: integrating color, texture, motion and shape," *Int. J. of Comp. Vision*, vol. 72, no. 2, pp. 195–215, 2007.

[7] S. Osher and J. Sethian, "Fronts propagating with curvature dependent speed: Algorithms based on hamilton-jacobi formulations," *J. of Comp. Phys.*, vol. 79, pp. 12–49, 1988.

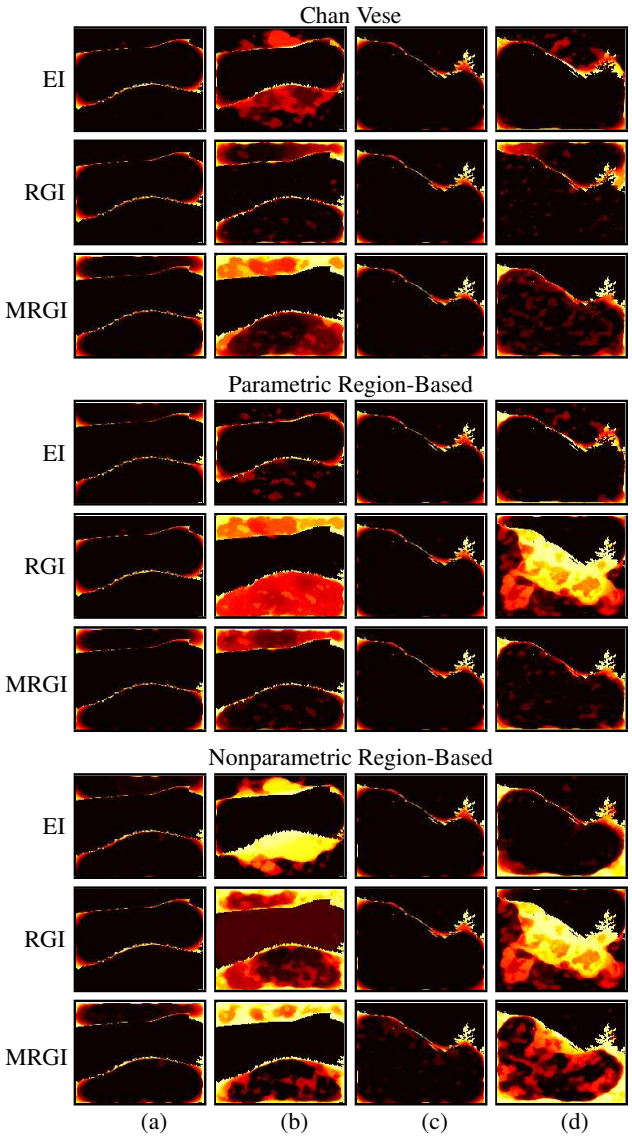

Fig. 5. Images showing the variation of the different methods and different initializations for $\mathbf{U_{3,2}}$, $\mathbf{U_{3,3}}$, $\mathbf{U_{4,2}}$, and $\mathbf{U_{4,3}}$ in Columns (a), (b), (c), and (d) respectively.

[8] V. Casselles, F. Catté, T. Coll, and F. Dibos, "A geometric model for active contours in image processing," *Numer. Math.*, vol. 66, pp. 1–31, 1993.

[9] R. Malladi, J. Sethian, and B. Vermuri, "A topology independent shape modelling scheme," in *Spie Conf. on Geometric Methods in Comp. Vision II*, vol. 2031, pp. 246–258.

[10] S. Zhu and A. Yuille, "Region competition: unifying snakes, region growing, and bayes/mdl for multiband image segmentation," *IEEE Trans. Pattern Anal. Mach. Intell.*, vol. 18, no. 9, pp. 884–900, 1996.

[11] T. Chan and L. Vese, "Active contours without edges," *IEEE Trans. Image Process.*, vol. 10, no. 2, pp. 266–277, 2001.

[12] K. Ohliger, , T. Edeler, S. Hussmann, A. Condurache, and A. Mertins, "A novel approach of initializing region-based active contours in noisy images by means of higher order statistics and dissimilarity," in *Int. Conf. on Mechatronics and Automation, 2010*, Xi'an, China, 2010, pp. 477–482.

[13] K. Ohliger, , T. Edeler, A. Condurache, and A. Mertins, "A novel approach of initializing region-based active contours in noisy images by means of unimodality analysis," in *IEEE 10th Int. Conf. on Signal Processing, 2010*, Beijing, China, 2010, pp. 885–888.

[14] N. Paragious and R. Deriche, "Geodesic active contours and level sets for the detection and tracking of moving objects," *IEEE Trans. Pattern Anal. Mach. Intell.*, vol. 22, no. 3, pp. 266–280, 2000.

[15] N. Paragios and R. Deriche, "Geodesic active regions: A new framework to deal with frame partition problems in computer vision," *J. of Visual Communication and Image Representation*, vol. 13, no. 1-2, pp. 249–268, 2002.

[16] G. Papandreou and P. Maragos, "Multigrid geometric active contour models," *IEEE Trans. Image Process.*, vol. 16, no. 1, p. 229, 2007.

[17] N. Paragios and R. Deriche, "Geodesic active regions and level set methods for supervised texture segmentation," *Int. J. of Comp. Vision*, vol. 46, no. 3, pp. 223–247, 2002.

[18] M. Rousson and N. Paragios, "Prior knowledge, level set representations & visual grouping," *Int. J. of Comp. Vision*, vol. 76, no. 3, pp. 231–243, 2008.

[19] J. Kim, J. Fisher, A. Yezzi, M. Cetin, and A. Willsky, "A nonparametric statistical method for image segmentation using information theory and curve evolution," *Image Processing, IEEE Transactions on*, vol. 14, no. 10, pp. 1486–1502, 2005.

[20] D. Freedman and T. Zhang, "Active contours for tracking distributions," *IEEE Trans. Image Process.*, vol. 13, no. 4, pp. 518–526, 2004.

[21] D. Comaniciu, V. Ramesh, and P. Meer, "Kernel-based object tracking," *IEEE Trans. Pattern Anal. Mach. Intell.*, vol. 25, no. 5, pp. 564–575, 2003.

[22] Y. Shi and W. Karl, "A real-time algorithm for the approximation of level-set-based curve evolution," *IEEE Trans. Image Process.*, vol. 17, no. 25, pp. 645–656, 2008.

[23] L. Dice, "Measures of the amount of ecologic association between species," *Ecology*, vol. 26, no. 3, pp. 297–302, 1945.